ON THE SPECTRAL DECOMPOSITION OF SKEWNESS IN CANONCIAL AND ACTUATED TURBULENT BOUNDARY LAYERS

S. Midya,
Institute for Flow Physics and Control
University of Notre Dame
Notre Dame, IN
Samaresh.Midya.1@nd.edu

F. O. Thomas*
Institute for Flow Physics and Control
University of Notre Dame
Notre Dame, IN
fthomas@nd.edu

S. V. Gordeyev
Institute for Flow Physics and Control
University of Notre Dame
Notre Dame, IN
sgordeye@nd.edu

ABSTRACT

The skewness of the streamwise velocity is an important parameter in turbulent boundary layer flows. It is intrinsically related to the mechanism of quadratic energy transfer between different scales of motion and has also been shown to be related to the modulation of near-wall turbulence by large scales. In this paper, the skewness in both a canonical and actuated zero pressure gradient turbulent boundary layer is spectrally decomposed via the real part of the bispectrum. It is shown that the real part of the bispectrum allows the individual triad interactions contributing to the skewness to be characterized. These measurements are presented for a range of wall-normal locations associated with positive, zero and negative skewness. The individual contributions are also summed to obtain partial and cumulative sums of the skewness as a function of frequency. Complementary conditional sampling measurements demonstrate that the main contribution to boundary layer skewness is intimately associated with ejection-sweep events and the degree of asymmetry of their characteristic velocity signatures. Actuation is used to document the influence of outer layer large-scale structures on the spectral content of skewness.

INTRODUCTION

It is clear that the skewness of the streamwise velocity fluctuations is an important parameter in turbulent boundary layers (TBL). In general, wall bounded turbulence is a multiscale phenomenon and there is a continuous exchange of energy between different scales of motion. The skewness is intrinsically related to the quadratic energy transfer mechanism between modes since only triadically coupled modes make non-zero contributions to the skewness (Duvvuri & McKeon, 2015). In the previously cited reference it is also shown that the skewness can provide the phase relation between triadically coupled modes. Skewness is also intimately related to the interactions between different spatial scales present in the turbulent flow. Hutchins and Marusic (2007a,b) demonstrated that near wall turbulence is modulated by the outer large-scale motions. This amplitude modulation of near wall turbulence was characterized by Mathis et al (2009, 2011). Their study correlated a low-pass filtered outer region signal with the envelope function of the near-wall, small-scale velocity fluctuations obtained via a Hilbert transform. The resulting profile of the normalized amplitude modulation correlation coefficient was found to bear a very strong resemblance to the corresponding wall normal skewness profile. Using a scale decomposed signal given by $u+ = u_L^+ + u_S^+$ where subscripts L and S denote large- and small-scale contributions, respectively, they showed that a significant contribution to the to the skewness is from the cross term between u_L and $(u_S)^2$.

Given this documented importance, this paper examines the spectral decomposition of the skewness in both a canonical and actuated zero-pressure gradient TBL at Re_θ = 1,770. This decomposition is achieved via the real part of the bispectrum and provides a direct measure of the modal contribution to the skewness at selected representative wall-normal locations. The relation between the skewness and the bispectrum is described in the following section.

THE SPECTRAL DECOMPOSITION OF SKEWNESS

Like the spectral decomposition of the second moment via the autospectral density, one can decompose the skewness in frequency domain using the third-order spectral estimate known as the bispectrum. The bispectrum captures the triadic interactions between the frequencies present in the flow. The bispectrum is defined as,

$$B_{XXX}\left(f_1^*,f_2^*\right)=E\left[\hat{X}^C_{f^*}\hat{X}_{f_1^*}\hat{X}_{f_2^*}\right]$$

where

$$f^*=f_1^*+f_2^*$$

Here, $E[\ ]$ denotes an expected value, $\hat{x}_{f_1^*}$ a temporal Fourier transform of a time series $x(t)$ and the superscript C denotes a complex conjugate. In the application of the bispectrum to be used in the boundary layer here, the frequencies have been normalized by the large eddy frequency ($f_i^* \equiv f_i\,\delta\,/U_\infty$). Owing to its symmetry properties (e.g Rosenblatt and Ness (1965), Kim and Powers 1979, Elgar (1987)) it is sufficient to compute the bispectrum for the triangular frequency domain

----
* Corresponding author

shown in Figure 1. This triangular region is associated with triad sum interactions. The correspodning two difference interactions involving the same wave triad would also map to the same point in this domain. For the triangular region shown in Figure 1, the third moment is related to the real part of the bispectrum by the relation (Rosenblatt and Ness (1965), Elgar and Guza (1985)),

$$E\left(u^3(t)\right)=12\sum_{f_1^*}\sum_{f_2^*<f_1^*}\mathrm{Re}\left(B_{xxx}\left(f_1^*,f_2^*\right)\right)+6\sum_{f_1^*}\mathrm{Re}\left(B_{xxx}\left(f_1^*,f_2^*\right)\right)$$

This equation can be normalized by u_{rms}^3 in order to directly relate the real part of the bispectrum to skewness. The real part of the bispectra to be presented were computed from velocity time-series signals normalized by u_{rms}^3.

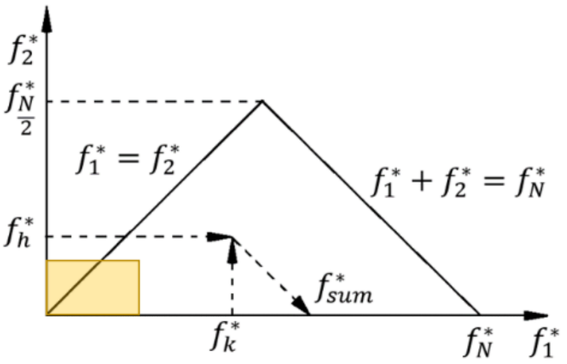

Figure 1. Region of computation of the auto-bispectrum. Only the sum interaction region is shown.

EXPERIMENTAL FACILITY

The experiments were conducted in a subsonic, open-return wind tunnel in the Hessert Laboratory at the University of Notre Dame. The wind tunnel has an inlet with a contraction ratio of 20:1. The inlet has a series of 12 turbulence management screens to condition the flow resulting in freestream turbulence levels of less than 0.1% for frequencies greater than 10 Hz. The test section is 0.61 m by 0.61 m in cross section and 1.83 m in length. A flat boundary layer development plate 2 meters in length with an elliptic leading edge covered with distributed sandgrain roughness was installed in the tunnel. The plate spanned the full width of the test section. Constant temperature hot-wire traverses confirmed canonical zero pressure gradient TBL development on the plate. Table 1 summarizes the boundary layer parameters measured at x =1.42 m downstream of the plate leading edge.

Table 1. Turbulent Boundary Layer Parameters

δ	U_∞	u_τ	C_f	H	Re_θ	Re_τ
35 mm	7.0 m/s	0.298 m/s	0.0037	1.3	1,770	690

The momentum thickness Reynolds number was purposely set sufficiently low that there was no energetic large-scale vortical structures in the outer region as occurs in higher Reynolds number TBLs. In order to introduce *highly organized* large-scale spanwise vorticity into the boundary layer, a plasma-based Active Large-Scale Structure Actuator (ALSSA) was developed and used (see Lozier et al, 2020, 2022). The ALSSA uses AC-DBD plasma to produce a pulsed jet that introduces organized large-scale coherent structures into the TBL. Figure 2 shows a schematic of the setup. The actuator consists of thin plate of streamwise length δ (the boundary layer thickness), spanwise length 8δ and maximum thickness of 0.05δ, with its trailing 0.3δ linearly tapered. The contoured elliptic leading edge of the plate was located at a streamwise distance of x =140 cm from the boundary layer development plate leading edge. The plate was placed at a wall normal location of h = 0.3δ ($h^+ = 200$). The spanwise length chosen ensured spanwise homogeneity of the vortical structures. The plate was made of Ultem (dielectric material) to facilitate the plasma generation. The DBD plasma was operated with a 4kHz carrier frequency with 32kV peak-to-peak voltage and was modulated with a square wave at a frequency of 80Hz ($f^* = 0.4$) with 50% duty cycle. This introduced a series of spanwise vortices at passage frequency $f^* = 0.4$ into the TBL at $y^+ = 200$. The resulting modal velocity is shown in Figure 10 of Lozier et al (2020, 2022).

For the canonical turbulent boundary layer at $Re_\theta = 1770$, the Reynolds number was sufficiently low that the pre-multiplied 1-D wavenumber spectra showed no dominant outer peak. In this manner, the ALSSA could be used to introduce periodic coherent structures into the outer region as described in Lozier et al (2021, 2022). This allowed examination of their influence on the nature and spectral decomposition of skewness.

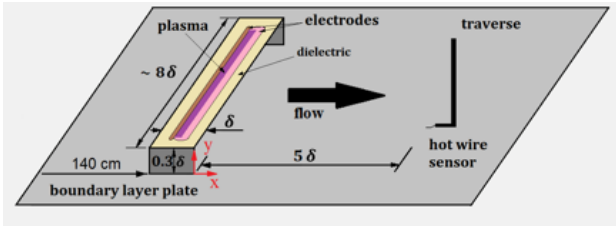

Figure 2. Schematic of the ALSSA actuator mounted on the boundary layer development plate.

Figure 3 compares skewness profiles for the canonical and plasma-actuated turbulent boundary layer cases. This figure shows similar skewness profile shapes for both cases. However, somewhat higher positive skewness occurs near the wall for the plasma actuated case. Both profiles reach near zero skewness at $y^+ = 15$ with the plasma actuated case showing greater negarive skewness in the lower logarithmic region.

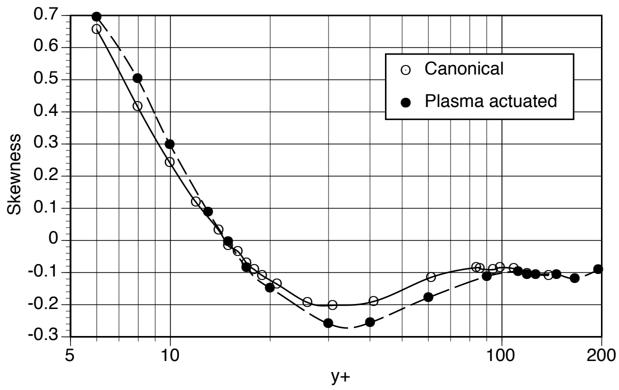

Figure 3. Skewness profiles for the canonical and plasma-actuated turbulent boundary layers.

SPECTRAL DECOMPOSITION OF SKEWNESS IN THE TURBULENT BOUNDARY LAYER

The location $y^+ = 8$ is selected as representative of the positive skewness that is observed in the near-wall region of turbulent boundary layers over a wide range of Reynolds numbers. The spectral decomposition for the canonical boundary layer case at this location is shown in Figure 4a. The real part of the bispectrum is presented in an f_1^*, f_2^*, sub-domain (highlighted by the yellow colored rectangular region in Figure 1) that is a smaller subset of the full domain in order to highlight the region of significant modal content. For all bispectral computations, a sampling frequency of 30 kHz ($f_{sample}^* = 150$), an FFT blocksize of 8192 and total 1300 blocks were used for the calculations. A series of convergence tests were performed in order to verify that all bispectra were fully converged (Midya, 2021)

The variable-interval-time-averaging (VITA) conditional sampling technique of Blackewelder and Kaplan (1976) was also applied to the time-series velocity fluctuations but a distinction was made in the conditional sampling algorithm between ejection-sweep (ES) events leading to positive versus negative skewness. The ES signatures that give rise to negative skewness will be denoted by -Ve and those giving rise to positive skewness are denoted +Ve. For comparative purposes, Figure 4b presents the probability density functions (PDF) at $y^+ = 8$ for VITA ES event frequency, f^*, that result in either positive or negative skewness. The PDF for positive skewness events is indicated in red while that associated with negative skewness is indicated in green and overlays the +Ve with sufficient transparency so that its PDF can still be discerned. It is quite clear that at $y^+=8$ positive skewness ES events are much more frequent which is fully consistent with the positive skewness shown in Figure 3 for the $y^+=8$ location.

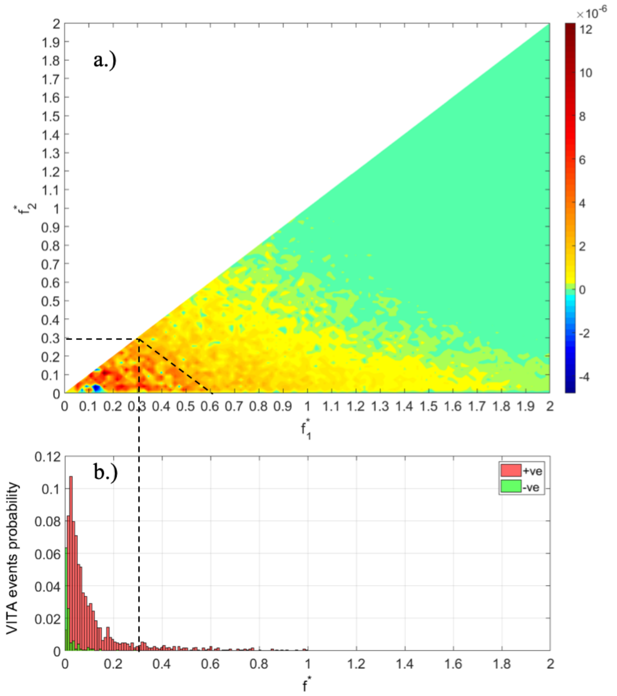

Figure 4. a) Spectral decomposition of skewness at $y^+=8$ for the canonical TBL. b) PDF of the frequency of positive (+Ve) and negative (-Ve) skewness producing E-S events.

Figure 4a shows that the most significant triad interactions contributing to positive near-wall skewness at $y^+ = 8$ involve f_1^* and $f_2^* < 0.3$. That is, the region of most significant triad interactions is bounded by $f_1^* + f_2^* = 0.6$ as indicated by the triangular region delineated by the dashed lines. Figure 4b shows this to corresponds to the frequency range contributing most to the probability density function for the frequency of +Ve burst events. Based on the VITA conditional sampling, the mean positive skewness event frequency at $y^+ = 8$ is approximately $f_{+ve}^* = 0.05$. It may be noted from Figure 4a that the highest peaks of the real portion of the bispectrum lie inside the dashed region with triad interactions that involve multiples of this frequency: $(i/2)\, f_{+Ve,1}^* + (j/2)\, f_{+Ve,2}^*$, $i = 2,3,4,5$ $j = 2,3,4,5$. Figure 4a also shows that weaker triad interactions involving $f_1^* = f_2^* < 0.7$, which conicides with the upper limit of frequency content of the PDF for VITA ES event frequency, also contribute to the positive skewness.

Figure 5a presents the spectal decomposition of skewness at $y^+ = 8$ for the ALLSA actuated TBL. Figure 5b presents the corresponmding PDFs at $y^+ = 8$ for VITA ES event frequency, that result in either positive or negative skewness. With actuation, the most probable frequency for positive and negative producing ES events is $f_{+ve}^* = 0.04$ and $f_{-ve}^* \approx 0.003$, respectively. These values are quite compaerble to that seen in the canonical case shown previsouly. As in the canonical TBL, the dominant triad interactions involve involve f_1^* and $f_2^* < 0.3$ as indicated by the dashed triangular region in Figure 5a. The peak triad interactions in this region are again associated with integer multiples of f_{+ve}^*. A main difference of the spectral decomposition for the actuated TBL are the indicated triad interactions associated with actuation frequency $f^* = 0.4$ and a range of frequencies extending to $f^* = 1.5$ as highlighted by the arrows in Figure 5a. These triad interactions are shown to also be associated with the production of positive skewness.

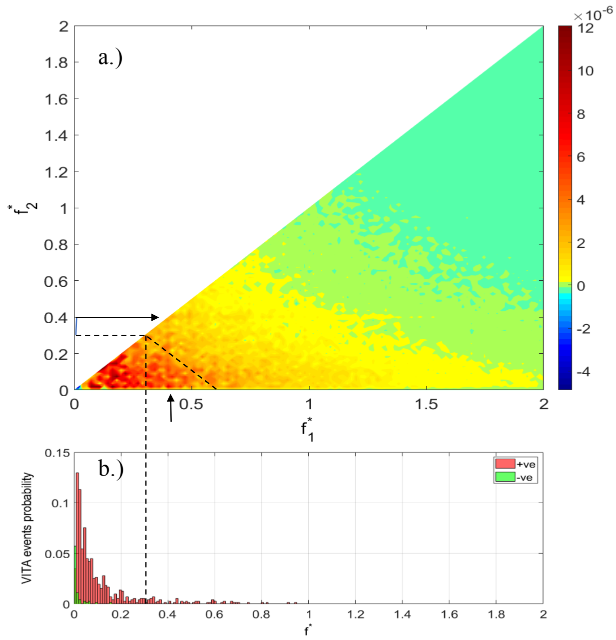

Figure 5. a) Spectral decomposition of skewness at $y^+=8$ for the actuated TBL. b) PDF of the frequency of positive (+Ve) and negative (-Ve) skewness producing E-S events.

As described earlier, a summation over the real part of the bispectrum recovers the skewness. Figure 6 shows the method of summation over the real part of the bispectrum. The frequency resolution, Δf_1^* and Δf_2^* of the bispectral plot are set equal. As shown in Figure 6a the area is divided using lines connecting $(i\,\Delta f_1^*, 0)$ and $(0, i\Delta f_2^*)$ (where $i = 1,2,..,N$). The sum is taken over the region between a pair of consecutive lines and is denoted by V_i (where $i = 1,2,..,N$). These values can then be plotted as a partial sum as shown in Figure 6b. The abscissa is denoted f_{12}^* and its resolution Δf_{12}^* equals Δf_1^*. Thus, the area under the curve of V_i recovers the skewness.

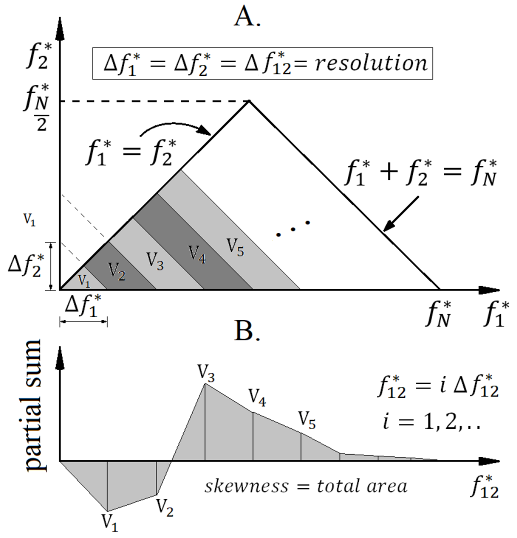

Figure 6. Summation over the real part of the bispectrum to recover skewness.

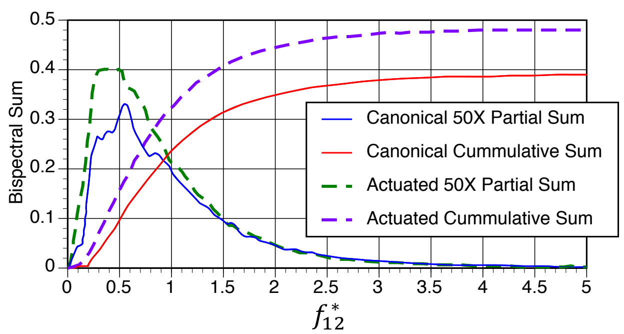

Figure 7. Partial and cumulative bispectral sums for the canonical and actuated TBL at $y^+ = 8$.

Figure 7 compares the partial and cumulative bispectral sums for the canonical and actuated TBLs at $y^+=8$. Both exhibit similar partial bispectral sum variations with f_{12}^*. The dominance of triad interactions producing positive skewness is readily apparent. The canonical case peaks near f_{12}^*= 0.6 and the actuated case near f_{12}^*=0.5. In both cases this is associated with the dominant triad interactions within the dashed regions shown in Figures 4a and 5a. The higher cumulative sum exhibited in the actuated case is associated with multiple triad interactions occurring for f_1^* and $f_2^* > 0.4$ associated with the imposed large-scale structures. Despite this, the similarity between canonical and actuated cases speaks to the primary role played by ES events in the near wall region.

Figure 8a presents the spectral decomposition of skewness at $y^+ = 15$ for the canonical TBL. The corresponding PDFs for the frequency of positive (+Ve) and negative (-Ve) skewness producing ES events is shown in Figure 8b. It is clear from this figure that at this wall normal location the relative frequency of both type of events is now quite comparable. More specifically, $f_{+ve}^* = 0.031$ and $f_{-ve}^* = 0.029$. This is consistent with the observation from Figure 3 that the skewness is nearly zero at this wall-normal location. Figure 8a shows that as before, the dominant interactions are clearly associated with the frequency range shown in the associated PDFs for +Ve and -Ve events ($f_1^*, f_2^* < 0.3$). Negative bispectral peaks are now present in this region for $f_1^* < 0.3$ and $f_2^* < 0.15$. Examination of the ordinate scale shows that the negative peaks clearly dominate the positive peaks in this region. Several discrete positive bispectral peaks are shown for $f_1^* > 0.3$ and $f_2^* = 0.05$. The f_2^* value corresponds to the f_{+ve}^* value observed at $y^+ = 8$ which suggests that these are a manifestation of comparatively rare, but high amplitude positive skewness producing ES events.

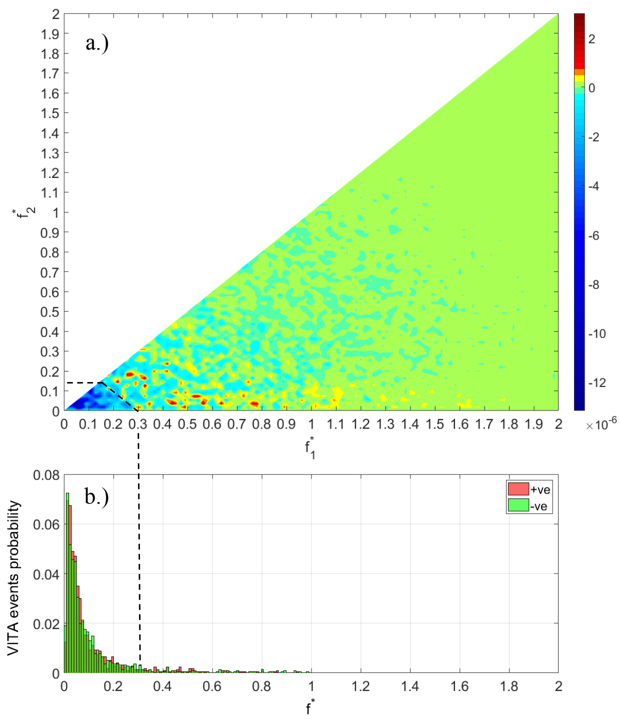

Figure 8. a) Spectral decomposition of skewness at y^+=15 for the canonical TBL. b) PDF of the frequency of positive (+Ve) and negative (-Ve) skewness producing E-S events.

Figure 9a presents the spectral decomposition of skewness at y^+ =15 for the actuated TBL. The corresponding PDFs for the positive and negative skewness producing ES events are shown in Figure 9b. As in the canonical flow the most probable frequencies for positive and negative skewness producing events are comparable: $f_{+ve}^* = 0.034$ and f_{-ve}^*= 0.038. These are also similar to the values observed in the canonical flow. As was the case for the canonical TBL, negative peaks dominate the bispectrum for $f_1^* < 0.3$ and $f_2^* < 0.15$. The influence of the ALLSA-imposed outer large-scale structures is also readily apparent. It is manifest in multipe positive skewness producing triad interactions between $0.04 < f_2^* < 0.4$ and a range of frequencies $0.4 < f_1^* < 1.2$ although the strongest occur for $f_1^* < 0.6$.

Figure 10 compares the partial and cumulative bispectral sums for the canonical and actuated TBLs at y^+=15. The dominance of the negative skewness producing triad interactions shown in the dashed triangular regions in Figures 8a and 9a is readily apparent and both the actuated and canonical partial sums show nearly identical strong negative peak values centered near f_{12}^*=0.2. The primary difference

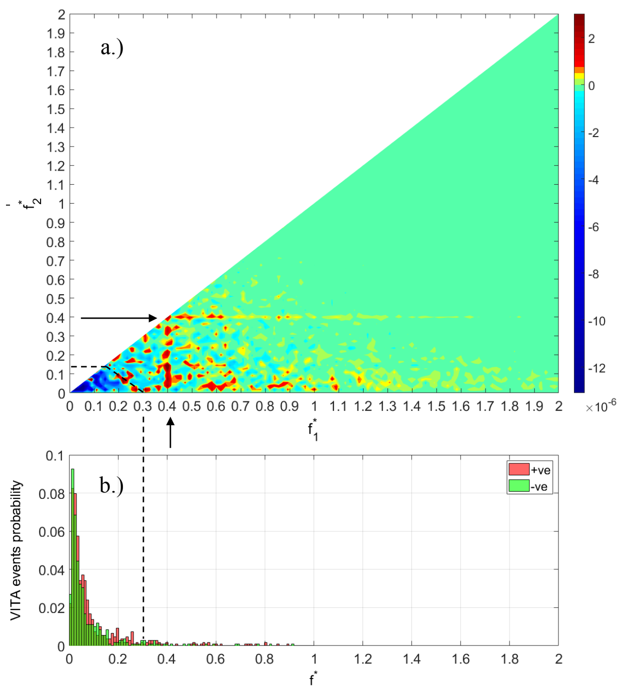

Figure 9. a) Spectral decomposition of skewness at y^+=15 for the actuated TBL. b) PDF of the frequency of positive (+Ve) and negative (-Ve) skewness producing E-S events.

between the two cases is associated with multiple positive skewness producing triad interactions between f_2^* = 0.4 and a range of frequencies extending to f_1^* = 1.2 for the actuated case. This gives rise to the positive peaks in the actuated case partial sum leading to nearly nearly zero skewness in the cumulative sum. In contrast, the canonical case cummulative sum remains negative. The picture that emerges once again from comparison of Figures 8, 9, and 10 is the dominant role played by ES events in determining the skewness. Although the outer large-scale strucures also have an influence, it is secondary as evidenced by comparison of the variation in partial and cumulative sums.

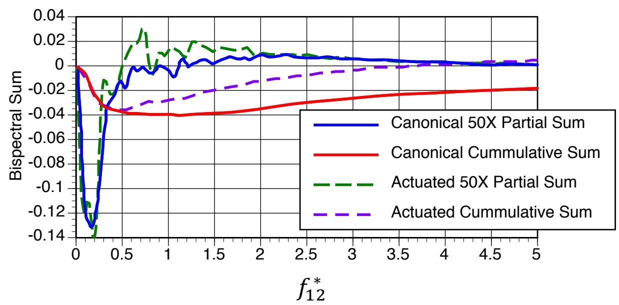

Figure 10. Partial and cumulative bispectral sums for the canonical and actuated TBL at y^+ =15.

The spectral decomposition of skewness for the canonical TBL at y^+ = 60 is shown in Figure 11a and now demonstrates a clear overall dominance of multiple triad interactions producing negative skewness. The corresponding PDFs obtained at y^+ = 60 for the frequency of both +Ve, positive and -Ve, negative skewness producing ES events are presented in Figure 11b. This figure shows the significantly increased frequency of negative skewness producing events relative to those producing positive skewness. The mean frequency for +Ve events is f^*_{+ve} = 0.049 and for -Ve events, f^*_{-ve} = 0.076 at this location. The dominant interactions shown in the spectral decomposition involve multiples of the mean frequencies for both +Ve and -Ve events with interactions producing negative skewness dominating.

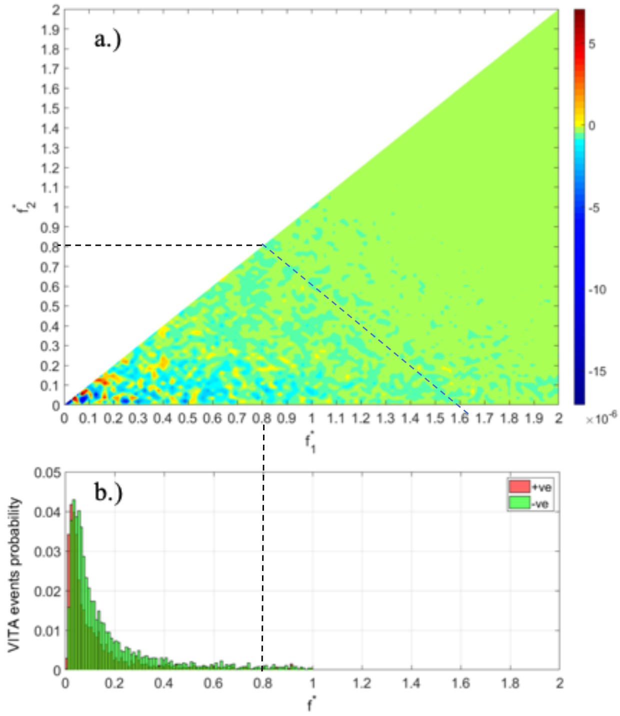

Figure 11. a) Spectral decomposition of skewness at y^+=60 for the canonical TBL. b) PDF of the frequency of positive (+Ve) and negative (-Ve) skewness producing E-S events.

Figure 12a presents the spectral decomposition of skewness for the actuated TBL at y^+ = 60. The corresponding PDFs for the frequency of ES events producing positive and negative skewness are shown in Figure 12b. As was the case in the canonical flow, the mean frequency of negative skewness eventsis f^*_{-ve} = 0.085 which exceeds that for positive skewness producing events which is f^*_{+ve}= 0.053 (very similar to the canonical case). Consistent with this, triad interactions associated with negative skewness dominate the spectral decomosition over the frequency band associated with the PDFs of ES events.

The effect of the actuated large-scale structures imposed by ALLSA is also now readlily apparent in the logarithmic region and gives rise to a range of triad interactions producing positive skewness for f_2^* < 0.4 and f_1^* > 0.4.

Figure 13 compares the partial and cumulative bispectral sums for the canonical and actuated TBLs at y^+=60. This location is within the lower logarithmic region of the mean velocity profile (the center of the logarithmic region is given by $y^+ = \sqrt{15\,Re_\tau} = 102$). In this case the influence of the introduced large-scale structures is quite significant. The canonical case is dominated by triad interactions producing negative skewness over a wide range in frequency. In contrast, the influence of the imposed large-scale vortical structures gives rise to a series of triad interactions (Figure 12a) that produces a positive peak in the partial skewness summation at $f_{12}^* = 0.4$. It is also apparent that the imposed structures exacerbate the negative triad interactions giving rise to two negative peaks in the cumulative sum centered near the frequencies $f_{12}^* = 0.26$ and 0.77, such that the cumulative sum for the actuated case is more negative than in the canonical flow. It is interesting to note that the negative peaks centered at $f_{12}^* = 0.26$ & 0.77 are, to good approximation, equal to $3f_{-ve}^*$ and $9f_{-ve}^*$, repectively and so are intimately tied to the ES process.

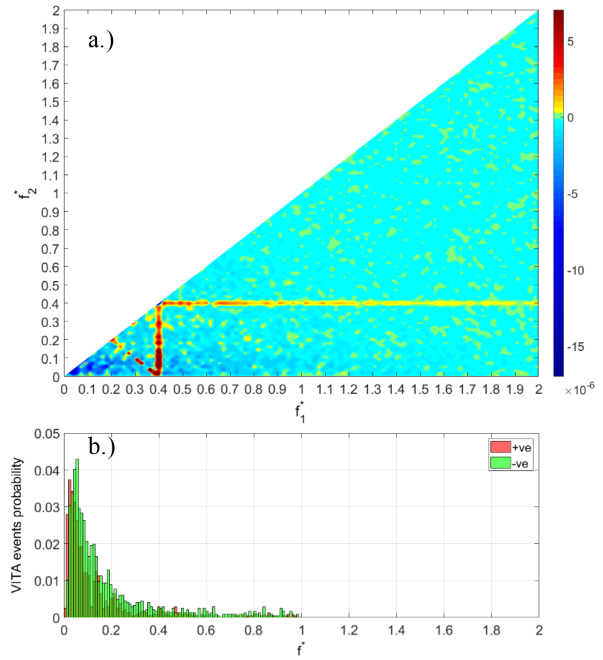

Figure 12. a) Spectral decomposition of skewness at y^+=60 for the actuated TBL. b) PDF of the frequency of positive (+Ve) and negative (-Ve) skewness producing E-S events.

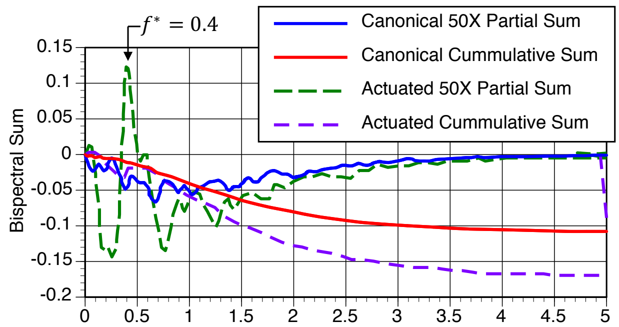

Figure 13. Partial and cumulative bispectral sums for the canonical and actuated TBL at y^+=60.

Figure 14 presents the phase-averaged skewness (mean removed) in the actuated boundary layer. Here u denotes the full signal, $\tilde{u}$ denotes the periodic modal component due to the imposed periodic actuation and u' the residual turbulence. This figure clearly shows that the artifically introduced outer large-scale structures at y^+=200 modulate the skewness consistent with the previously presented bispectra. Although this effect extends to near the wall, it is much more pronounced in the logarithmic region. Hence, as shown in the spectral decomposition measurements, even in the actuated boundary layer, the near wall skewness is largely dominated by discrete ES events associated with buffer layer streamwise vorticity. This explains the overall similarity between the partial and cumulative bispectral sums shown for locations y^+ = 8 (Figure 7) and y^+ = 15 (Figure 10). In contrast, in the logarithmic region at y+ = 60 (Figure 13) there is condiderable disparity in the partial and cumulative bispectral sums for the canonical and actuated cases.

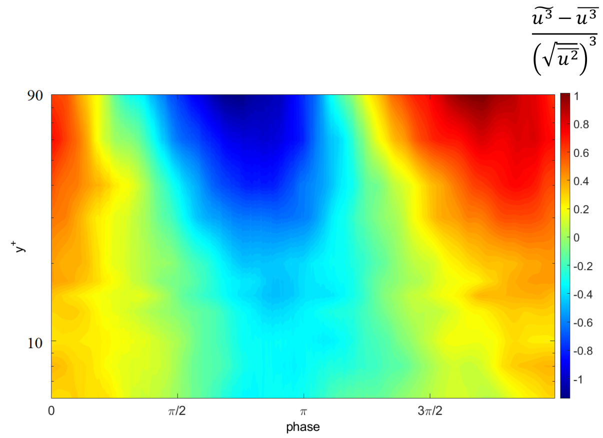

Figure 14. Phase-averaged skewness (mean removed) in the actuated turbulent boundary layer.

CONCLUSION

The real part of the bispectrum is used to spectrally decompose the skewness of streamwise fluctuating velocity in both a canonical zero pressure gradient TBL and for the case in which the ALLSA actuator (Lozier et al, 2020, 2022) introduces spanwise oriented periodic vortical motions into the TBL at y^+ = 200. In both cases Re_θ = 1,770. This Reynolds number is sufficiently low that a naturally occurring dominant outer turbulence intensity peak does not exist in the 1D pre-multiplied streamwise wavenumber spectrum (Midya, 2021). Comparison of the spectral decomposition for the natural and actuated turbulent boundary layer is performed at three wall-normal locations: y^+ = 8, which represents a region of positive skewness in the near-wall region; y^+ = 15 which corresponds to the wall normal location of peak turbulence intensity and for which the skewness is near zero; y^+ = 60 which represents the lower logarithmic region (the log region geometric center is located at y^+ = 102).

Supporting conditional measurements show that the triad interactions responsible for near-wall skewness are intimately tied to the frequencies associated with positive and negative skewness producing ejection-sweep events. This suggests the important role played by buffer layer streamwise vortices in near-wall TBL skewness. Furthermore, the imposition of large-scale vortical structures into the logarithmic region via ALLSA has little effect on the spectral distribution of skewness at y^+ = 8 and only a modest effect at y^+ = 15 with the observed triad interactions remaining dominated by those associated with positive or negative skewness producing ejection-sweep events. In contrast, the effect of the actuation becomes quite significant at y^+ = 60 where triad interactions associated with the presence of coherent structures with passage frequency f^* = 0.4 become readily apparent and significantly effect the skewness. Modes associated with the outer layer organized structures are shown to undergo triad interactions with those associated with ejection-sweep events to give rise to enhanced negartive skewness in the actuated case.

The important role played by buffer layer streamwise vorticity in TBL skin friction drag has been demonstrated by Kim (2011). The wall-directed fluid motion created by these vortices gives rise to so-called "splatting" events that increase viscous drag. Their presence is also manifest in the positive skewness that dominates the near-wall region of TBLs over a wide range of Reynolds numbers. The results of this study show that this positive skewness is associated with triad interactions involving modes at multiples of the ejection-sweep frequencies associated with positive skewness producing events. In a similar manner the near zero skewness occurring farther from the wall has been shown to be associated with triad interactions producing negative skewness that is associated with low speed fluid directed away from the wall.

There has emerged consensus that there is an autonomous, near-wall cycle responsible for the generation and growth of buffer layer streamwise vortices as described in Jimenez & Moin (1991), Waleffe et al. (1993), Hamilton et al. (1995), Jimenez & Pinelli (1999) and Schoppa and Hussain (2002) among others. The results of this study support a near-wall autonomous mechanism associated with the production of buffer layer vortices whose role in near-wall skewness is shown to dominate as evidenced by the similarity in the partial and cumulative spectral skewness sums for the canonical and actuated cases at representative locations $y^+ = 8$ and $y^+ = 15$. In addition to this, the artificially imposed large-scale structures are shown to also influence the skewness, as has been shown in previously cited studies involving higher Reynolds number TBLs containing naturally occurring energetic large-scale structures in the outer region. The influence of these large-scale structures on skewness is clear from the partial and cumulative skewness spectral sums obtained at each location but occurs most prominently at $y^+ = 60$ (shown in Figure 13). The results of this study also show that the effect of modulation by outer large-scale structures on skewness grows with distance from the wall. The increased effect of large-scale modulation with distance from the wall is readily apparent in the phase averaged skewness shown in Figure 14.

AKNOWLEDGEMENT

This work is supported by Office of Naval Research, Grant number N00014-18-1-2534.

REFERENCES

Blackwelder, R.F., Kaplan, R.E. On the wall structure of the turbulent boundary layer, 1976, J. Fluid Mech., Vol. 76, pp. 89-112.

Duvvuri, S., and McKeon, B., “Phase relations in a forced turbulent boundary layer: implications for modelling of high Reynolds number wall turbulence”. Philos Trans A Math Phys Eng Sci., 375(2089), 20160080, 2017.

Elgar, S., 1987, Relationships Involving Third Moment and Bispectra of a Harmonic Process, IEEE Transactions on Acoustics and Signal Processing, Vol. ASSP-35, No. 12, pp 1725-1726.

Hamilton, J., Kim, J. & Waleffe, F., 1995, “Regeneration mechanisms of near wall turbulence structure,” *J. Fluid Mech.*, Vol 287, pp.317–3489

Hutchins and I Marusic. Evidence of very long meandering features in the logarithmic region of turbulent boundary layers. *J. Fluid Mech.*, 579:1–28, 2007a.

N. Hutchins and I. Marusic. Large-scale influences in near-wall turbulence. *Philos. Trans. R. Soc. A*, 365(1852):647–664, 2007b.

Jimenez, J. & Moin, P., 1991, “The minimal flow unit in near wall turbulence,” *J. Fluid Mech.*, Vol 225, pp. 213–240.

Jimenez, J. & Pinelli, A., 1999, “The autonomous cycle of near-wall turbulence,” *J. Fluid Mech.* Vol. 389, pp. 335–359.

Kim, J., “Physics and control of wall turbulence for dragreduction,” Phil. Trans. R. Soc. A 369, 1396–1411, 2011.

Kim, Y. C. and Powers, E. J., "Digital Bispectral Analysis and Its Applications to Nonlinear Wave Interactions," in *IEEE Transactions on Plasma Science,* vol. 7, no. 2, pp. 120-131, June 1979, doi: 10.1109/TPS.1979.4317207.

Lozier, M., Thomas, F.O., and Gordeyev, S. 2020. Streamwise Evolution of Turbulent Boundary Layer Response to Active Control Actuator. AIAA SciTech Forum, AIAA Paper 2020-0097.

Lozier, M., Thomas, F. O. and Gordeyev, S.V.,“Experimental Studies of Boundary Layer Dynamics via Active Manipulation of Large-Scale Structures,“ Procedings of the 12th Turbulent Shear Flow Phenomena (TSFP12), Osaka, Japan, 2022.

Mathis, R., Hutchins, N., and Marusic, I., 2009, Large-scale amplitude modulation of the small-scale structures in turbulent boundary layers, J. Fluid Mech., Vol. 681, p. 311.

Mathis, R., Marusic, I., Hutchins, N. and Sreenivasan, K. R., 2011, The relationship between the velocity skewness and the amplitude modulation of the small scale by the large scale in turbulent boundary layers, Physics of Fluids, 23, 121702.

Midya, S.,“On the spectral decomposition of skewness of streamwise velocity in a zero pressure gradient turbulent boundary layer,“ PhD Thesis, University of Notre Dame, 2021.

Rosenblatt, M.; Ness, J. W. Van. Estimation of the Bispectrum. Ann. Math. Statist. 36 (1965), no. 4, 1120--1136. doi:10.1214/aoms/1177699987.

W. Schoppa & Hussain, F., Coherent structure generation in near-wall turbulence. J. Fluid Mech., 453:57–108, 2002.

Waleffe, F., Kim, J. & Hamilton, J., 1993, “On the origin of streaks in turbulent boundary layers,” in *Turbulent Shear Flows 8*, pp. 37–49.